JOURNAL OF MASS SPECTROMETRY, VOL. 31, 602–615 (1997)

Injection of Externally Generated Ions into an Increasing Trapping Field of a Quadrupole Ion Trap Mass Spectrometer

Vladimir M. Doroshenko and Robert J. Cotter*
Middle Atlantic Mass Spectrometry Laboratory, Department of Pharmacology and Molecular Sciences, The Johns Hopkins University School of Medicine, 725 N. Wolfe Street, Baltimore, Maryland 21205, USA

Trapping ions injected into a quadrupole ion trap (QIT) by increasing the trapping r.f. voltage on a ring electrode is an effective and widely recognized method of interfacing an ion trap with pulsed ion sources such as matrix-assisted laser desorption/ionization (MALDI). In this paper, the problem of mass discrimination during the injection and trapping of ions by the increasing r.f. field was studied both experimentally and by numerical simulation using SIMION software. For a MALDI/QIT interface design with a remote external ion source described here, experiments with polyethylene glycol (PEG 1000 and PEG 1500) showed little mass discrimination for trapping ions in a wide mass range (500–2000 Da) for a broad range of experimental conditions, which include kinetic energies of 5–40 eV for the injected ions and an r.f. voltage of 400–4000 V_{0-p} amplitude ramped at a rate of 30–140 V_{0-p} μs^{-1}. In the numerical simulation, complex and sharp dependences of the trapping efficiency on the phase of the r.f. voltage and initial kinetic energy of ions were observed. However, after averaging over the r.f. phase and over a reasonable range of kinetic energy, the simulation resulted in relatively constant and high values for the trapping efficiency (normally 0.2–0.3) for any mass and kinetic energy considered, which are consistent with the weak sensitivity to injection parameters observed in the experiment. A simple model for the qualitative description of ion injection and trapping is suggested that relies on phase interaction of injected ions with the r.f. field rather than on collisions with the buffer gas molecules to decrease the ion kinetic energy.

J. Mass Spectrom. **32**, 602–615 (1997)
No. of Figs: 15 No. of Tables: 0 No. of References: 54

KEYWORDS: quadrupole ion trap; matrix-assisted laser desorption/ionization; ion injection; ion trapping; mass discrimination

INTRODUCTION

The Paul quadrupole ion trap (QIT)[1] is a means for long-term storage of ions placed inside the trap cell. Since its invention, methods for placing ions inside the trap have been and are among the most important goals for investigation.[2,3] These investigations were greatly accelerated by the introduction of the mass-selective instability mode of operation and subsequent commercialization of ion trap mass spectrometers.[4] In the first commercial ion trap instruments, ions were generated inside the trap by electron impact (EI) or chemical ionization (CI) methods. However, in situ ionization methods are limited to only relatively volatile analyte species. Moreover, the control of EI collision parameters in the presence of the strong r.f. electric field inside the trap is a difficult task. For this reason and because of the demand for interfacing with modern desorption ionization methods, external ion injection methods have been developed,[5] including those for interfacing the QIT with a Cs^+ secondary ion mass spectrometric (SIMS) source,[6] atmospheric pressure glow discharge (APGDI),[7] electrospray (ESI),[8] direct laser desorption (LD)[5,9,10] and matrix-assisted laser desorption/ionization (MALDI).[11–15] The major problem for all methods of external ion introduction is that ions which have been injected usually have too much energy to be trapped.

For continuous ionization methods such as SIMS, APGDI and ESI, the common method used for introduction of external ions injects ions into an active trapping field created by a constant r.f. voltage and subsequently reduces the kinetic energy of the ions by a dissipative process, usually via collisions with buffer gas molecules. This method has been discussed theoretically,[16–18] including a recent report of an ion injection simulation,[19] and has been well reviewed.[2,3,20,21] The main drawback of the method is its low trapping efficiency, which is about 0.2% at a pressure of 1 mTorr (1Torr = 133.3 Pa)of helium buffer gas.[19] Additionally, the efficiency of trapping is mass dependent.

The major approaches to the external introduction of ions produced in pulsed ion sources (such as LD or MALDI) are shown in Fig. 1. Ions may be desorbed near the internal surface of the ring electrode [radial introduction, Fig. 1(a)][9,10,12,13] or one of the end-cap electrodes [axial introduction, Fig. 1(b)].[22] Ions may also be formed in a remote ion source and be transmitted into the trap through a hole in one of the electrodes using ion optics [Fig. 1(c)].[5,11,14,15] A fiber optics guide

* Correspondence to: R. J. Cotter.
Contract grant sponsor: National Institute of Health: Contract grant number: R01 RR08912.

CCC 1076–5174/97/060602–14 $17.50

Received 15 January 1997
Accepted 14 February 1997

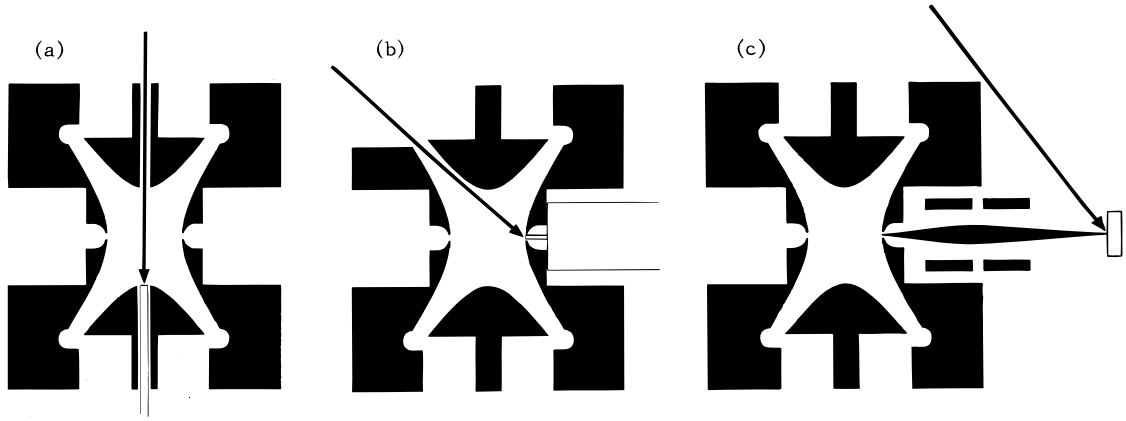

Figure 1. Different schemes for external introduction of ions produced by direct LD or MALDI methods.

can be used to deliver laser power to the target.[14,15] Additionally, McIntosh *et al.*[23] have designed an interface using a fiber optics guide without any ion optics, placing the sample at a 1 cm distance from the end-cap electrode. The cases shown in Fig. 1(a) and (b), in which ions are formed near or at the boundary of ion trap cavity, are characterized as an external introduction, because ions must still overcome the potential barrier to reach the center of the trapping field. Then, as in the case shown in Fig. 1(c), their kinetic energy must be reduced.

As in the case of continuous ion sources, ions formed by LD and MALDI may be injected into a constant r.f. trapping field and their kinetic energy reduced through collisions with the buffer gas, as was described in the first reports on interfacing MALDI[11–15] or LD[5,9,10] with QIT. However, pulsed ion sources provide an opportunity for methods of ion trapping other than the introduction into a constant r.f. potential. One such approach reduces the ion potential energy by pulsed operation of an ion trap.[3] In this method the trapping field is turned on after the ions reach the center region of the trap, by synchronizing the switching of the r.f. voltage with ion introduction. This method of trapping ions by gating the r.f. voltage has been extensively studied theoretically.[24–29] However, its practical use seems to be limited by low r.f. voltages and reports on its use are very rare.[30]

An alternative method was developed in our laboratory for trapping MALDI ions[22,31,32] and independently by Eiden and co-workers[33,34] for an LD ion source and involves gradual increasing of the trapping r.f. voltage during introduction of ions into the trap. This method incorporates some features of both methods discussed above, because ions are introduced into an active r.f. field, while the strength of that field is built around the ions about the time that they arrive at the center of the trap, by synchronizing the r.f. voltage ramp with ion introduction. At the same time, this method does not require fast switching of the r.f. voltage and, thus, is applicable for experiments involving high mass analysis where a high r.f. voltage is utilized. The length of time for ramping the r.f. voltage is determined by LCR circuitry used in the r.f. voltage generator[22] and is normally in the range 50–175 μs.

A related dynamic trapping method has been developed for external injection of ions,[19,35] and involves the use of a pulsed retarding electric field for deceleration and trapping of the injected ions. The retarding field is created inside the trap by applying an appropriate d.c. voltage pulse to the end-cap electrodes. This d.c. retarding voltage is much easier to pulse in comparison with the r.f. trapping voltage. However, the method is applicable only for ion beams of very short duration, as has been reported for incident ion beams lasting about 0.2 μs.[35]

At present, all of the geometries for ion introduction shown in Fig. 1 have been utilized with ion injection into an increasing trapping field, i.e. radial introduction,[33] axial introduction[22] and injection from the remote ion source.[36] The major experimental results reported for this method of ion introduction in the case when ions are formed at the boundary of the ion trap cavity have been limited to studies of the dependences of ion abundance upon the time and phase of laser firing, the r.f. voltage amplitude and buffer gas pressure. No direct measurements of the trapping efficiency have been available, although Garrett et al.[37] observed that this method gives approximately an order of magnitude improvement in signal levels over methods in which ions were injected into the constant trapping potential. (Measurements of the trapping efficiency by Qin and Chait[36] did not include ion losses on the trap electrodes and reflection at the entry to the trap which were shown to be important in the current work.) It has been shown that ions can be trapped at very low pressures, close to that of residual gases.[22,34] A strong dependence of the signal upon the phase of laser firing was observed in one report,[34] while another report[22] showed no such dependence. This can be attributed to different rates of ramping of the r.f. voltage in these experiments, as well as to the different initial ion kinetic energy distributions of ions formed in MALDI and LD ion sources. Finally, a study of the dependence of the ion signal upon the r.f. voltage level and time of the laser firing revealed that the trapping efficiency is mass dependent.[34] Additionally, no systematic investigations of this case using numerical or other theoretical methods have been done, although some initial attempts toward the numerical simulation of ion injection into the increasing trapping field were made for qualitative analysis of the results of the experiment.[34]

In this work, we extended our method of ejection of ions into an increasing trapping field to the case of ions

generated in a remote ion source [Fig. 1(c)]. A similar type of MALDI/QIT interface was successfully utilized by Qin and Chait[36] for the characterization of proteins with high sensitivity. In contrast to the present work, they used a trapping r.f. waveform containing both an increasing and decreasing r.f. field. The generation of ions in the remote ion source has obvious advantages because of the possibility for using sample arrays and fast switching to other ion sources. Our goal was to achieve mass-independent and highly efficient trapping of ions from a remote MALDI ion source and to describe the parameters which are most important for trapping. The method of numerical simulation using SIMION software[38] was used throughout this work for calculating the trapping efficiency and explaining the experimental results.

EXPERIMENTAL

Ion trap mass spectrometer

Experiments were carried out using an extensively modified Finnigan MAT (San Jose, CA, USA) ion trap detector (ITD) described in detail elsewhere.[39,40] The resonance ejection technique was used for extending the mass range by applying an a.c. ejection voltage from a Wavetek (San Diego, CA, USA) Model 95 arbitrary/function generator to the end-cap electrodes. MALDI using the fourth harmonic ($\lambda = 266$ nm) laser pulse of $\sim$10 ns duration from a Quantel International (Santa Clara, CA, USA) Model YG660-10 Q-switched Nd:YAG laser was used for production of ions from an external source. In addition, the instrument utilizes several features that have been described previously, including increased efficiency for trapping MALDI ions by increasing r.f. voltage,[22] linear calibration in the resonance ejection mode of operation using amplitude modulation of the ejection voltage,[41] a broadband excitation technique designed for the unit resolution ion isolation in the range up to 1600 Da using 'stretched-in-time' excitation waveforms[39] and pulsed introduction of heavy gas used in tandem mass spectrometric (MS/MS) experiments for improving the collision-induced dissociation(CID) efficiency and to allow a low-mass cut-off level for fragment ions analyzed.[40] The ion trap assembly was placed inside a two-section coffin vacuum chamber in which the ion trap and electron multiplier sections were pumped differentially by two turbomolecular pumps (Model TPH 330 (Balzers, Hudson, NH, USA) and Model TMP 150 (Leybold, Export, PA, USA).

Trapping r.f. and ejection a.c. voltage amplitudes were controlled externally using 12-bit analog outputs from a National Instruments (Austin, TX, USA) Lab PC+ multifunction plug-in board connected to the computer. The generation of the control voltage pattern during acquisition scanning was sampled synchronously with the acquisition of the data using a Lab PC+ analog input connected to the detector of the ion current at the exit of the ion trap. Broadband waveforms for the excitation and isolation of ions inside the trap were generated by two Quatech (Akron, OH, USA) WSB-100 waveform synthesizer plug-in boards with an on-board WSB-A12M 12-bit resolution analog module connected to the computer. Two WSB-100 boards were operated in a master/slave mode to provide the total waveform memory of 64K points of 16 bit length. Twelve bits of each point of the WSB-100 memory were used to generate the analog broadband signal while the other four bits could be used as digital lines to control external devices. The procedure for designing the excitation broadband waveforms was described earlier.[39] TrapWare software (designed in-house) was used for data acquisition and for controlling the instrument and additional hardware.[39,41] TOFWare, a WINDOWS-based program available from ILYS Software (Pittsburgh, PA, USA), was used for data processing and plotting.

MALDI/ion trap interface

In contrast to our previous work, in which MALDI ions were generated near the end-cap or ring electrode surface inside the trap, ions were produced outside the ion trap, injected through a hole in the entrance end-cap electrode and trapped by increasing of the trapping voltage during ion injection.[22]

The actual r.f. voltage profile used for trapping ions in our instrument is shown in Fig. 2. This waveform corresponds to the r.f. voltage applied to the ring electrode from 0 V to $V_{r.f.}$ and was recorded on the oscilloscope using a small capacitive divider (50 pF to 0.01 μF, where 50 pF is the approximate capacitance between end-cap and ring electrodes). The small voltage surge at the beginning of the waveform corresponds to the time (t_{laser}) of laser firing. The laser can be fired at any time within this waveform and can be synchronized with the r.f. voltage phase.[12] The middle part of the waveform (from $\sim$7 to 35 μs) is approximately described as a linearly increasing r.f. voltage originating at the time point t = 0 in Fig. 2. The settling time for the r.f. voltage is about 50 μs. This is about three times smaller than the settling period in the unmodified instrument, owing to changes in the values for capacitors on the Analog board of the ITD r.f. voltage generator.[22]

Using SIMION software, the ion injection scheme was designed to match the parameters of the trapping r.f. voltage waveform. A typical simulation for the injection scheme used is shown in Fig. 3. The sample probe voltage (+20 V for positive ions in Fig. 3) determines the ion injection kinetic energy at the entrance to the trap which is a hole of 1.2 mm diameter in the end-cap electrode held at 0 V during ion injection. The laser beam (not shown in Fig. 3) was focused on to the probe at the incident angle of $\sim$45° by a 50 cm focal length UV quartz lens. The probe can be rotated around the symmetry axis and moved in a horizontal direction so that any point on the probe surface within a circle of $\sim$5 mm diameter can be illuminated by the focused laser beam. Two electrostatic lenses (with potentials of −250 and −10 V in Fig. 3) focus the ions desorbed by the laser beam to the trap entrance. The distance from the probe tip to the trap entrance is about 51 mm. The trajectories of a group of ions of m/z 1000 having initial kinetic energies of 1 eV and desorbed over an angle

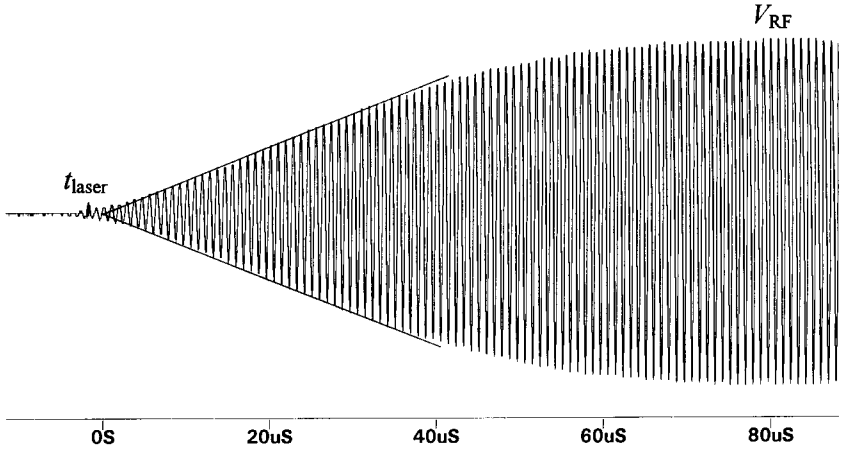

Figure 2. R.f. voltage profile used in experiments for trapping ions.

range from −45 to 45° normal to the probe surface are shown in Fig. 3. Potential contours are shown through every 50 V. Time markers (vertical lines across the ion trajectories in Fig. 3) are drawn every 1 μs. Total time of flight of ions m/z 1000 is about 15 μs, which is comparable to the r.f. voltage rise time in Fig. 2.

Ions not trapped passed through the trap during the injection period and were detected by an ETP Scientific (Auburn, MA, USA) Model AF612 electron multiplier located near the exit end-cap electrode. The signal from the multiplier was observed on a LeCroy (Chestnut Ridge, NY, USA) Model 9400A oscilloscope and was used for a qualitative analysis of the trapping process.

Operational procedures

Each single-scan experiment began with the firing of the laser. Desorbed ions were then injected into the trap and trapped by increasing the r.f. voltage, which was ramped from about zero at the time of laser firing to the settling value of $V_{r.f.}$. The settling r.f. voltage $V_{r.f.}$ was 20–60% of the maximum value $V_{r.f.,max} \approx 7.5$ kV_{0-p} (zero to peak) and was reached within about 50–60 μs. Typical ion injection times, from the time that ions were formed until the time that ions entered the trap, was about 15 μs. Following a period of cooling (20–30 ms), the broadband pulse was applied to eject low-mass ions ($m/z < 600$) and to reduce possible space charge effects.[2] After low-mass ejection and a second cooling period, the mass spectrum was recorded by scanning the r.f. voltage at a rate of 1000 Da s^{-1} using the resonance ejection technique. (Only singly charged ions are considered in this work and, thus, daltons (Da) are used here equally with m/z units). The frequency of the ejection a.c. voltage was 137.6 kHz if the mass interval did not exceed 1750 Da and 68.8 kHz if a higher mass range was to be recorded. The resonance ejection voltage was

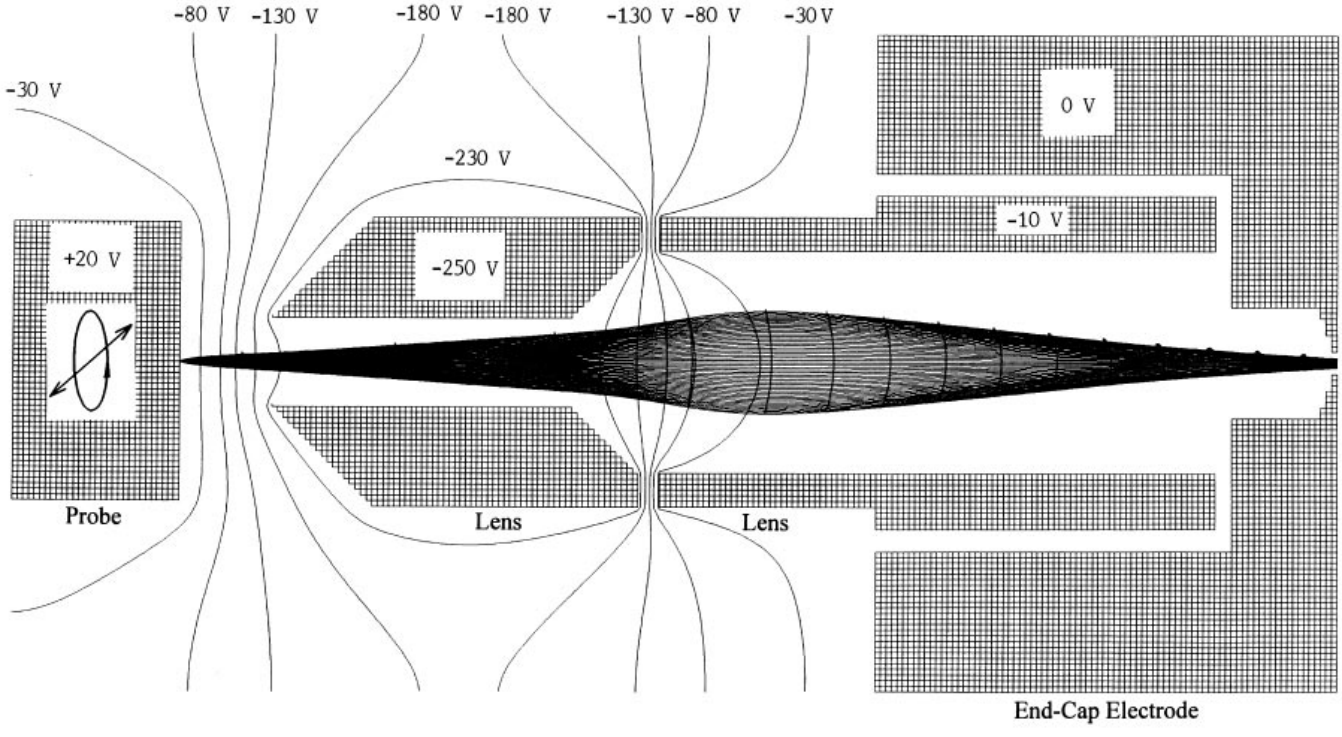

Figure 3. MALDI/ion trap interface used for ion injection with the trajectories for m/z 1000 ions having an initial kinetic energy of 1 eV calculated using the SIMION program. Markers along the trajectories are drawn every 1 μs.

also scanned, with its amplitude to be proportional to the ejected mass (with 6 V_{0-p} corresponding to m/z 1297). Mass spectra were produced by averaging ~150 spectra from the individual scans.

Nicotinic acid (Aldrich, Milwaukee, WI, USA) was used as the MALDI peptide matrix. It was prepared as a saturated solution in 2:1 chloroform–methanol, deposited on the stainless-steel probe in an amount of 10–20 μl and fast dried in a flow of air at room temperature. Aqueous solutions of 10–100 pmol poly(ethylene glycol) PEG 1000 or PEG 1500 (Sigma, St Louis, MO, USA) in amounts of 3–4 μl were deposited on the matrix and dried in the vacuum. Each sample was used to produce thousands of single laser shot spectra by moving the sample probe within a ~20 mm^2 area.

THEORETICAL

Numerical simulation

The results of the experiments were analyzed and interpreted using numerical simulation with SIMION software.[38] The real geometry of the standard Finnigan ion trap electrodes was used in these calculations. For these purposes, the dimensions of the electrodes were determined with an accuracy of ~0.1 mm, including flanges, holes, grooves, etc. Exceptions were holes in the flanges of the end-cap and ring electrodes. The exit end-cap electrode was replaced by one identical with the entrance end-cap (having a single hole aperture), since we utilized the axial symmetry case.

A program was written to simulate ion motion in the r.f. field in which the r.f. voltage amplitude profile in Fig. 2 was assumed to depend upon $V_{r.f.}$ only[34] and was approximated with an accuracy of ~2–3% by the expression

$$V = V_{r.f.}\left\{a - \frac{b}{1 + \exp[c(t + d)]}\right\} \quad (1)$$

where (for the time t shown in Fig. 2 and expressed in μs) the parameters a, b, c and d are equal to 1.0321, 1.1142, 0.0876371 and −23.1193, respectively.

In real experiments there are many initial parameters affecting the final trajectory of an injected ion. We approximated the real case by a beam of ions initially moving in a direction parallel to the symmetry axis. That is, we did not consider ions moving along inhomogeneous electrostatic fields created by ion optics elements (see Fig. 3) but started our calculations at the final stage of the ion injection (several millimeters before ions enter the trap) where the r.f. field strength is close to zero and the ion beam can be approximated by a group of ions moving parallel to each other. This is a good approximation of the experiment and greatly simplifies the numerical integration needed to find the trapping efficiency averaged over the initial ion parameters. Among the independent parameters of the numerical model were: the initial radial position ρ and kinetic energy ε_{kin} of an ion, the ion mass m, the time of the ion injection t_{inj} (or the time of laser firing t_{laser}), the settling r.f. voltage amplitude $V_{r.f.}$ and the initial r.f. voltage phase θ.

In this approximation, whether an ion is trapped or not depends upon the start time, the initial position of the ion on a planar surface orthogonal to the direction of ion flight, its kinetic energy and the phase of the r.f. voltage. We can also assume that ions are uniformly distributed in the initial planar surface. This is good approximation if one takes into account that MALDI ions are formed with a broad distribution of the kinetic energies[42–47] and ions with initial energies other than shown in Fig. 3 will be even more disfocused. In this case the trapping efficiency $P_{\varepsilon\theta}$ for ions starting at a point ds on an initial surface s and having initial energy ε_{kin} can be calculated using the following equation:

$$P_{\varepsilon\theta} = \frac{\int_s P_{\varepsilon\theta s} j_s \, ds}{\int_s j_s \, ds} \quad (2)$$

where j_s is the ion density at the initial planar surface and $P_{\varepsilon\theta s}$ is equal to 1 or 0 depending on whether ions are trapped or not. Additionally, by convention we only consider ions passing through the hole of the radius ρ_0 in the end-cap electrode and, thus, the trapping efficiency can be written as

$$P_{\varepsilon\theta} = \frac{1}{\pi\rho_0^2}\int_0^{\rho_0} 2\pi\rho P_{\varepsilon\theta s} \, d\rho \quad (3)$$

We used a numerical method to calculate the integral (3) by dividing the radial interval (0, ρ_0) into 12 equal parts. The error of integration was estimated to be <10%.

Simple estimations show that because of the initial energy distribution of ions in our experiments, the group of ions of the same m/z entering the trap extends over a time interval which is larger than the r.f. voltage cycle of 0.908 μs. Thus, the trapping efficiency can be averaged over the r.f. voltage phase θ (for θ expressed in radians):

$$P_\varepsilon = \frac{1}{2\pi}\int_0^{2\pi} P_{\varepsilon\theta} \, d\theta \quad (4)$$

Equation (4) is a good practical approximation because ions having small differences in initial kinetic energy experience large differences in r.f. voltage phase at the entrance into the trap.

Pseudopotential approximation

In some cases the motion of ions in an inhomogeneous r.f. field can be represented as a superposition of two motions having different time-scales. One of these is a simple oscillatory microscopic motion at the fundamental r.f. frequency, which appears as a ripple on the other smoother macroscopic trajectory governed by the inhomogeneous properties of the r.f. field. This approximation is known as a pseudopotential well approximation for a quadrupole ion trap.[48] In the case of grounded end-cap electrodes the approximation is valid for Mathieu parameters $q_z < 0.4$, and results in

two-dimensional harmonic motion of ions in a parabolic pseudopotential well having depths D_z and D_ρ in the z and ρ directions, respectively ($a_z = 0$):

$$D_z = \frac{eV^2}{2mr_0^2\Omega^2}$$

$$D_\rho = D_z/2 \tag{5}$$

where e is ion charge, r_0 is the radius of the ring electrode and Ω is the radial frequency of the r.f. voltage.

Equations (5) are valid for a pure quadrupole r.f. field. The field inside the real ion trap is far from ideal, due to the stretched and truncated geometry of the electrodes and holes in the end-cap electrodes. In the general case of a sinusoidal r.f. field the pseudopotential $U(x, y, z)$ can be written as[49]

$$U(x, y, z) = \frac{eE_0^2(x, y, z)}{4m\Omega^2} \tag{6}$$

where $E_0(x, y, z)$ is the amplitude of the r.f. electric field strength at particular space point. Equation (6) was used in our work to calculate the pseudopotential field distribution in the real ion trap. First, the SIMION program was used to calculate a real potential distribution inside the trap. Then, a program written in-house was used to calculate the distribution of the electric field $E_0(\rho, z)$ and the pseudopotential $U(\rho, z)$. Calculated values of $U(\rho, z)$ were packed and written to the file in the SIMION format. Thus, the pseudopotential field could be used by the SIMION program for ion trajectory experiments and graphical presentation.

RESULTS AND DISCUSSION

Trapping of ions according to the pseudopotential approximation

This approximation is known to be valid inside the trap for $q_z < 0.4$.[2] Unfortunately, ions spend a large part of the time during injection in areas far from the center of the trap, where the applicability of the approximation is in doubt. However, because of the simplicity of this approach, it was one of the goals of our experiments to explore the limits of this approximation.

The pseudopotential field distribution inside a stretched ion trap, calculated according to Eqn (6) for the case of $D_z = 10$ V, is shown in Fig. 4. Isopotential lines are drawn every 2 V with zero pseudopotential at the center of the trap. One can see that the depth of the pseudopotential well in the radial direction is about 3.9 V, which is much less than the 5 V predicted by Eqns (5). This is due primarily to the stretched geometry of the trap. In the axial direction the well depth is also shallower in comparison with the 10 V corresponding to an ideal quadrupole field. This results from the presence of holes in the end-cap electrodes. The field is highly disturbed near the holes and this can influence the process of injection and ejection of ions through the holes. The pseudopotential field distributions along the z-axis for the stretched and unstretched geometry are compared in Fig. 5, with the pseudopotential barrier higher for the stretched trap geometry. This means that the electric field strength E_0 near the end-cap electrodes is larger in the case of the stretched geometry.

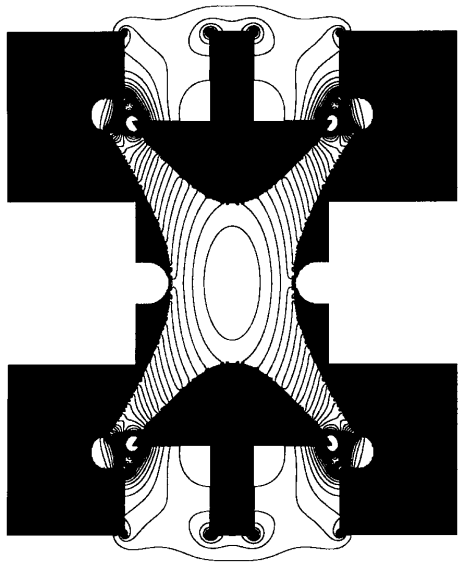

Figure 4. Pseudopotential field distribution inside the stretched ion trap.

In the pseudopotential approximation approach to ion injection, ions have to overcome an initial barrier (shown in Fig. 5) to enter the trap. One can therefore expect that the difference between the energy of an ion and the barrier height will also affect the trapping efficiency and the smaller difference is preferable for trapping.

As one can see from Eqns (5), the pseudopotential barrier height is proportional to the square of the r.f. voltage V applied to the ring electrode and inversely proportional to the mass-to-charge ratio m/z. If the r.f. voltage amplitude increases proportionally to the time t (as in the case of the middle part of the real r.f. wave-

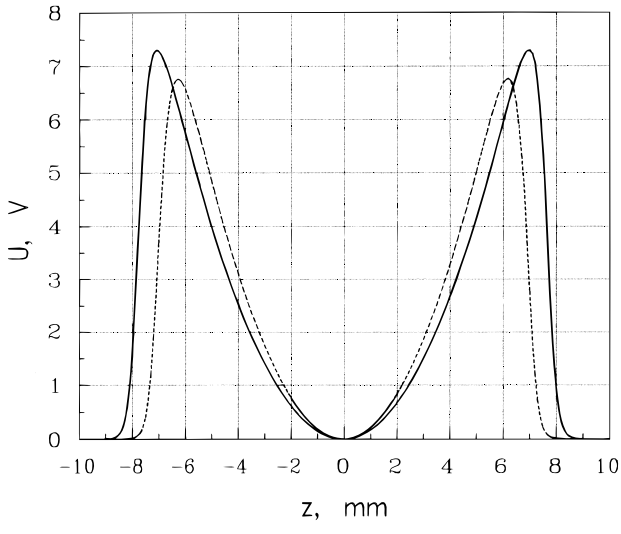

Figure 5. Pseudopotential field distribution along the z-axis for an ion trap with stretched (solid line) and unstretched (dashed line) geometry.

form shown in Fig. 2) and the mass-to-charge ratio for ions entering the trap through the hole in the end-cap electrode is proportional to the square of the time (as is the case in a time-of-flight mass spectrometer,[50]) then the ions entering the trap will experience the same pseudopotential barrier. For ions having the same initial kinetic energy this means that the conditions of injection will be the same for all ions. This occurs in the case of the ion injection interface shown in Fig. 3, because ions of different mass-to-charge ratio (having initial kinetic energies determined primarily by the potential on the sample probe) follow the same trajectory but have different flight time proportional to their mass-to-charge ratios: $t \propto (m/z)^{1/2}$.

Thus, if the laser fires at time $t = 0$ in Fig. 2, then ions entering the trap during the time interval 7–35 μs (corresponding to the linearly increasing part of the r.f. voltage waveform) experience the same pseudopotential barrier. The validity and limits of this approach must, of course, be tested experimentally because the pseudopotential approximation may not work near the holes in the end-cap electrodes.

Experimental study of the mass discrimination for the injection of external ions

Initially, we tested the pseudopotential approximation approach using poly(ethylene glycol) mixtures with average molecular masses of 1000 Da (PEG 1000) and 1500 Da (PEG 1500), and with the laser fired at $t = 0$. Because the molecular distributions for these compounds are well known and have been accurately characterized by MALDI,[51] these samples provide an excellent opportunity to study the mass discrimination of our MALDI/QIT interface. The MALDI mass spectrum of PEG 1000 obtained with the potential of the sample probe at 21 V and the r.f. voltage $V_{r.f.} = 0.21V_{r.f., max}$ ($V_{r.f., max} = 7500\ V_{0-p}$), is shown in Fig. 6. MNa^+ ions are observed in the spectrum. The mass resolution is about 3500 at m/z 1000 and the isotopic structure of the peaks is well resolved. However, because the isotopic contributions have some effect on the peak shapes we smoothed the spectra over the mass range using TOFWare to produce the isotopically unresolved spectrum (shown as the inset in Fig. 6) which reveals a molecular mass distribution close to the expected one.[52]

In Fig. 7, the mass spectra of PEG 1500 obtained at low [Fig. 7(a)] and high [Fig. 7(b)] laser power are shown. Again, MNa^+ ions are observed and the molecular mass distribution is improved after smoothing [insets in Fig. 7(a) and (b)]. Along with the basic molecular ion distribution one can also observe fragments formed during laser desorption of the sample, with higher abundance fragments occurring at higher laser power [Fig. 7(b)]. The fragments are singly charged ions, as follows from the study of an isotopic distribution of the fragment ion peaks (not shown). Two sets of fragments are formed which are shifted relative to the basic distribution by −2 Da (this set is too close to the basic distribution to be seen clearly in Fig. 7, but it is recognizable when fragment and parent ions are of comparable abundance) and −18 Da. These two sets of ion fragments correspond to cleavages of different ester bonds in the backbone of the parent ions. The convolution of the initial mass distribution for the parent ions and possibly the different probabilities of cleavages of

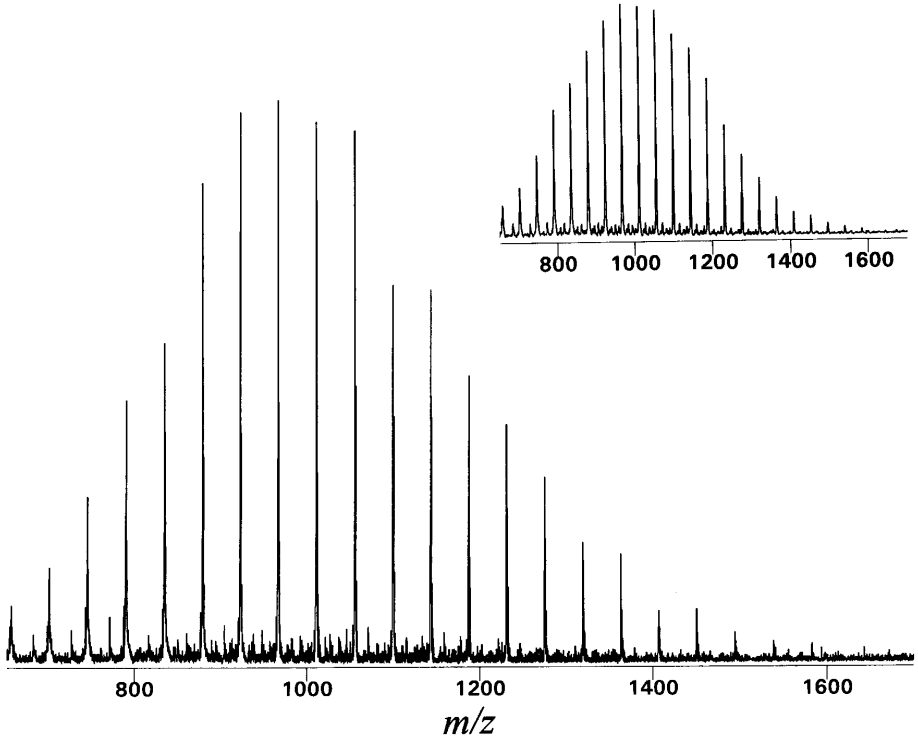

Figure 6. MALDI mass spectrum of PEG 1000 obtained when the time for laser firing $t = 0$, with a potential on the sample probe of 21 V and settling r.f. voltage $V_{r.f.} = 0.21V_{r.f., max}$. The spectrum in the inset is the same data smoothed to produce peaks with unresolved isotopic structure.

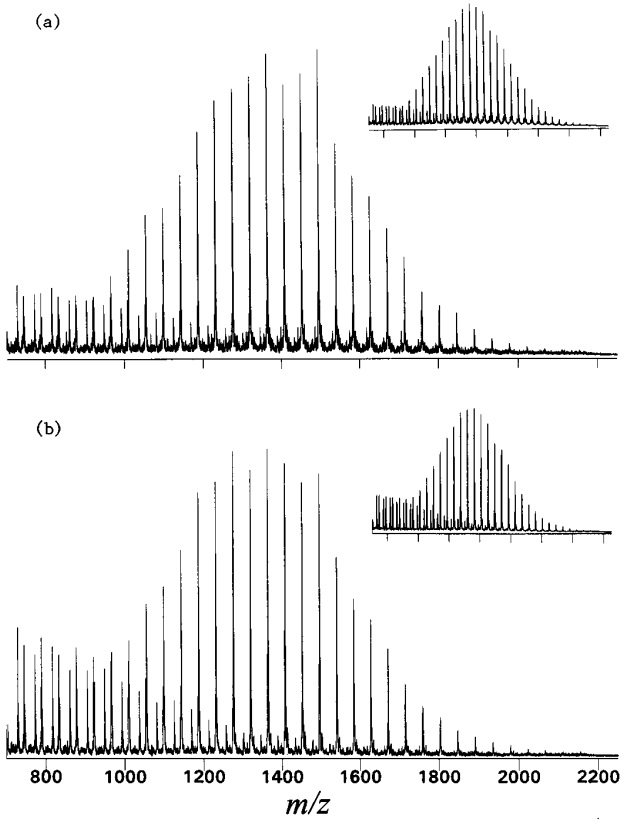

Figure 7. MALDI mass spectra of PEG 1500 obtained at (a) low and (b) high laser power, with the time for laser firing $t = 0$, the potential on the sample probe of 21 V and the settling r.f. voltage $V_{r.f.} = 0.21V_{r.f.,\,max}$. The spectra in the inset are the same data smoothed over to produce peaks with unresolved isotopic structure.

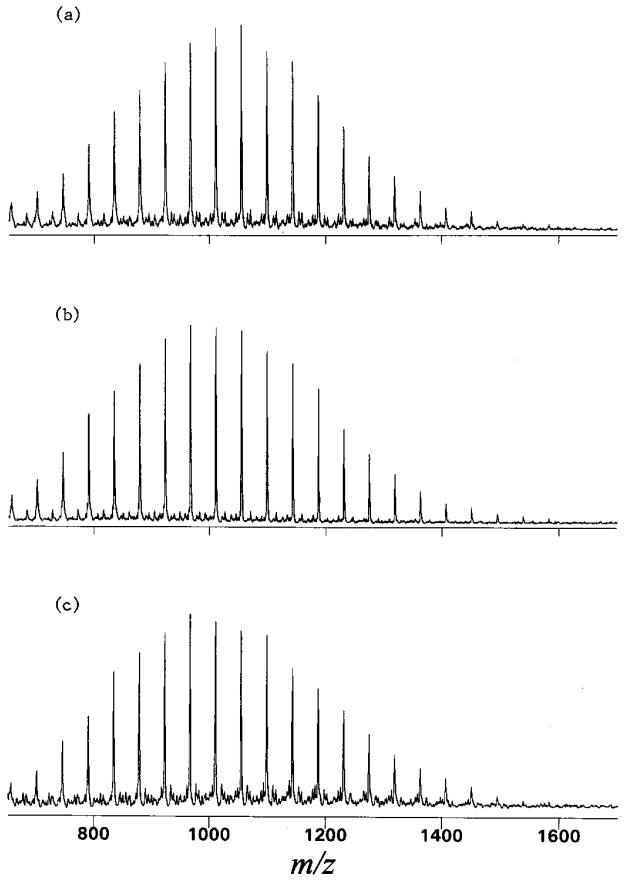

Figure 8. PEG 1000 molecular mass distribution for different times of laser firing: t_{laser} = (a) −7.5 , (b) 0 and (c) 7.5 μs. $V_{r.f.} = 0.21V_{r.f.,\,max}$; the potential on the sample probe was 21 V.

ester bonds along the ion backbone account for the lower mass distribution for the fragment ions in Fig. 7.

In order to study our approach further, we carried out additional experiments in which the time of laser firing was varied, i.e. $t_{laser} = -7.5$, 0 and +7.5 μs. The results of these experiments for PEG 1000 are reported in Figs 8 and 9, where the smoothed MALDI mass spectra are presented for the settling r.f. voltage $V_{r.f.} = 0.21V_{r.f.,\,max}$ and $0.5V_{r.f.,\,max}$, respectively. If the pseudopotential approximation is valid in the case of ion injection then one could expect some changes in the intensity and/or slope of the molecular mass distribution when the laser is fired earlier or later than the optimal time $t = 0$. However, the molecular mass distributions are similar to those observed in Fig. 6 except for that obtained at very high r.f. voltage V during injection, $V_{r.f.} = 0.5V_{r.f.,\,max}$ and the laser firing at $t_{laser} = +7.5$ μs [Fig. 9(a)]. For this case a very low-intensity spectrum is observed because most of the ions are rejected by the r.f. field. The other spectra in Figs 8 and 9 are of comparable intensity despite the fact that the pseudopotential well depth (at $t = 0$) is different for the cases shown in Figs 8 and 9 ($D_z = 3$ and 17 eV, respectively).

In another series of experiments, we changed the potential on the probe, thus changing the initial kinetic energy of ions. In some experiments this required retuning the voltages on the ion lenses to obtain better focusing of ions on to the entrance hole. Using PEG 1000 at a settling r.f. voltage $V_{r.f.} = 0.5V_{r.f.,\,max}$, we obtained similar molecular mass distributions of comparable intensities while changing the voltage on the sample probe from 5 to 40 V (data not shown), a range of voltages from considerably less to considerably larger than the pseudopotential well depth ($D_z = 17$ eV in this case).

Thus, while we obtained good molecular mass distributions for PEG 1000 and 1500 firing the laser at $t = 0$ that are consistent with the pseudopotential approximation approach, results obtained at earlier and later times over a broad range of experimental conditions cannot be explained by this approximation without invoking additional factors.

Numerical simulation

An example of our simulation of ion injection and trapping is shown in Fig. 10, where 25 ions of m/z 750 uniformly distributed along the radius ρ and having the initial kinetic energy $\varepsilon_{kin} = 18$ eV are injected into an increasing r.f. field ($V_{r.f.} = 0.5V_{r.f.,\,max}$, $\theta = 225$). Plots of these trajectories begin at a planar surface located 5 mm in front of the entrance hole, where the r.f. field strength according to the data in Fig. 5 is equal to zero. Additionally, the start time and consequently the initial r.f. voltage amplitude and phase for ion motion in Fig. 10 (and later figures unless specified otherwise) was chosen

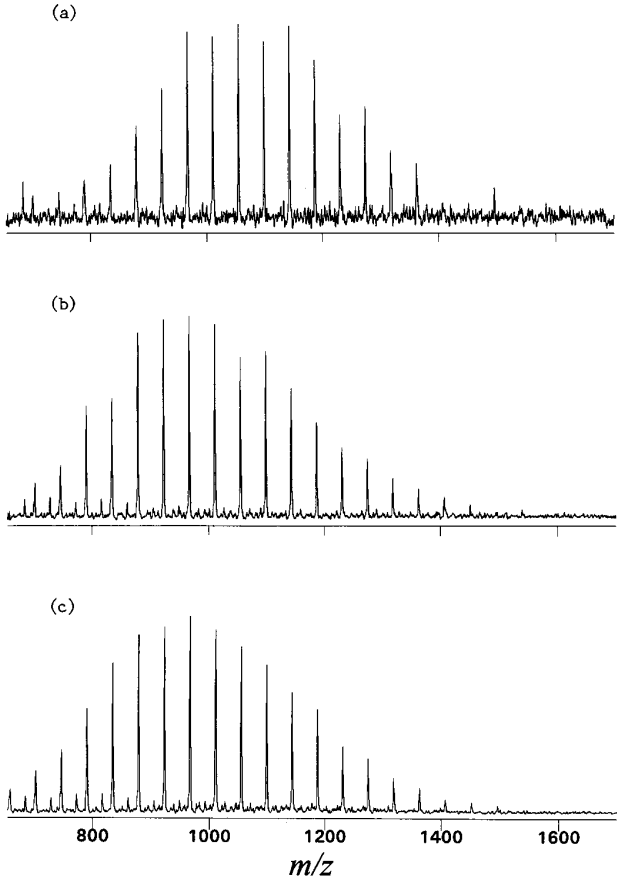

Figure 9. PEG 1000 molecular mass distribution for different times of laser firing (a)–(c) as in Fig. 8. $V_{r.f.} = 0.5V_{r.f., max}$; the potential on the sample probe was 21 V.

to correspond to the injection time in the experiments ($t_{inj} = 15$ μs for m/z 1000 ions, see Fig. 3). The trajectories were calculated for the first 40 μs and for collisionless conditions. If the ions perform several oscillations in axial and radial directions during this time then they are trapped. This is always true (as checked by calculating the trajectories for typical cases over 1000 μs time periods) in the case in which the trapping field is built up by increasing the r.f. voltage during injection. This is also true for most ion trajectories in the case of ion injection into the constant r.f. field, especially if one takes into account the damping of oscillations in the longer time-scale due to the collisions with the buffer gas molecules (our calculations for this case can be considered at least as a good estimation). We do not consider the collisions with helium buffer gas molecules because they are not important in this time-scale and because the trapping efficiency will only be higher if collisions are taken into account.[19] The trajectories of 25 ions initially equally spaced along a hole diameter are shown in Fig. 10 but one has to keep in mind that ions starting at different radii have to be taken with different weights as described by Eqn (3) to calculate the trapping efficiency. In the case of Fig. 10 all ions pass through the hole and most of them are trapped, while a few ions pass through the trap and others strike the surface of the exit end-cap electrode. If the contribution according to Eqn (3) is taken into account then there are ten times fewer ions passing through the trap than striking the surface of the exit end-cap electrode. In other cases (not shown), ions can be reflected by the r.f. field at the entrance to the trap. For these reasons, the trapping efficiency cannot be determined by measuring only the number of trapped ions and the number passed through the trap.[36]

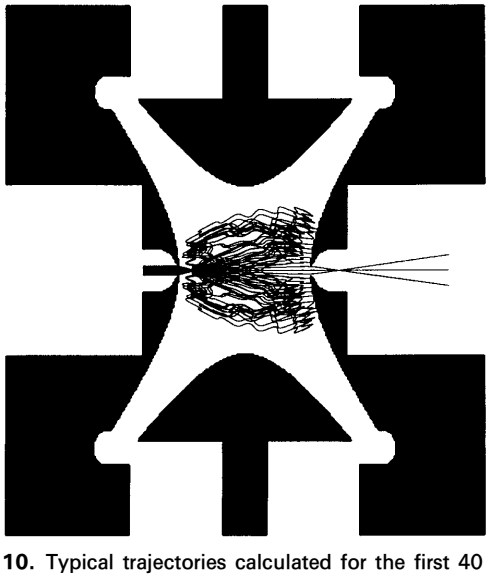

Figure 10. Typical trajectories calculated for the first 40 μs after injection of 25 ions of m/z 750 into an ion trap with an increasing r.f. potential (r.f. waveform as in Fig. 2; $V_{r.f.} = 0.5V_{r.f., max}$). Ions are flying from left to right.

An important feature of the injection and trapping process represented in Fig. 10 is the essentially two-dimensional ion motion (in axial and radial directions), which is due to the hole in the entrance end-cap electrode and cannot be observed if the hole is not taken into account.[19,34] The hole acts as a lens, effectively scattering ions entering the trap over the larger trap volume. Its role is positive for the trapping process because deflected ions can be reflected near the exit end-cap electrode by a higher pseudopotential barrier (see Fig. 4; in most cases the pseudopotential approximation is applicable for the motion inside the trap). Knowing the fate of all ions injected into the trap (as in the example case for 25 ions in Fig. 10), one can calculate the trapping efficiency $P_{\varepsilon\theta}$ using Eqn (3).

Figure 11 gives a general presentation of the dependence of the trapping efficiency $P_{\varepsilon\theta}$ on the r.f. voltage phase θ and initial kinetic energy ε_{kin} for injection of an m/z 1000 ion into an increasing r.f. field with $V_{r.f.} = 0.5V_{r.f., max}$. The surface $P_{\varepsilon\theta}(\varepsilon_{kin}, \theta)$ is very uneven with numerous peaks, ridges and valleys. Note that the height of the peaks and ridges is approximately unity for the entire range of kinetic energy considered (from 8 to 40 eV). The dependence of $P_{\varepsilon\theta}$ upon the r.f. voltage phase θ is shown in Fig. 12 for the cases of $\varepsilon_{kin} = 21$ and 40 eV, exhibiting complex and different phase behavior of $P_{\varepsilon\theta}$ for $\varepsilon_{kin} = 21$ and 40 eV.

The dependence of the trapping efficiency $P_{\varepsilon\theta}$ upon a broader range of initial kinetic energy is shown in Fig. 13 (solid curve), and we also calculated the trapping efficiency for injection of the same ions into a constant r.f. field (dashed curve). In the latter case, the amplitude of the constant r.f. voltage on the ring electrode was chosen to be equal to that of the increasing r.f. field at the time when ions were near the hole. This means that

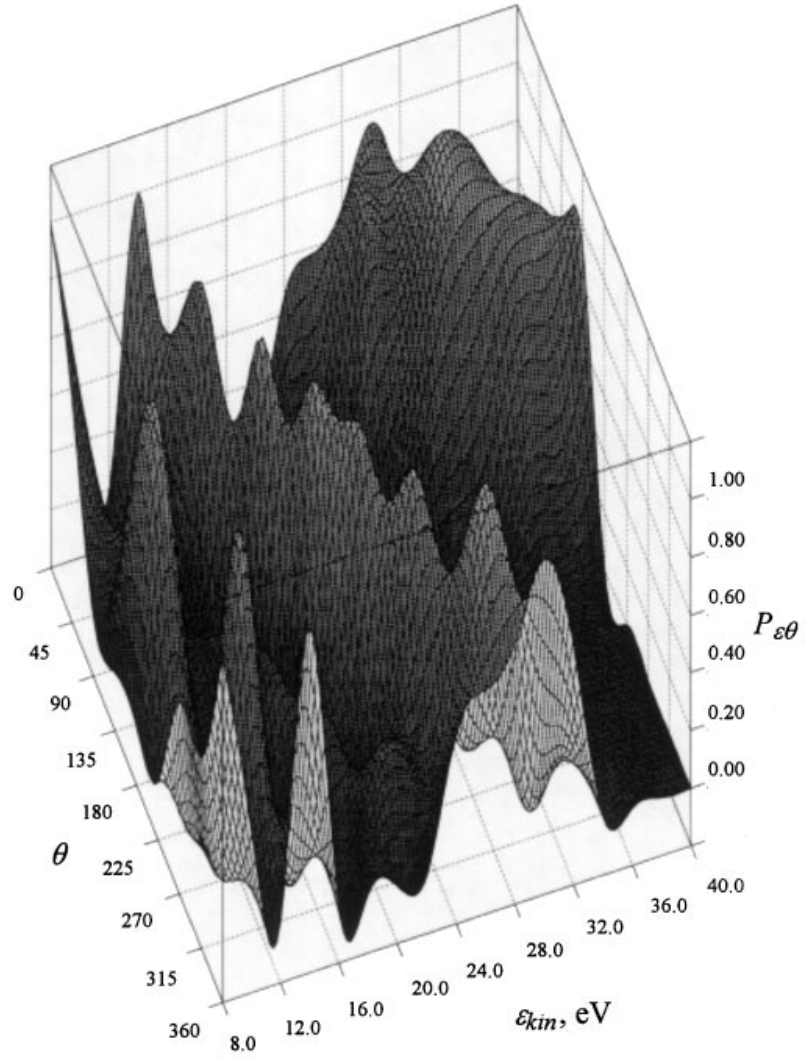

Figure 11. Dependence of the trapping efficiency $P_{\varepsilon\theta}$ during injection of m/z 1000 ions into an ion trap with increasing r.f. field (r.f. waveform as in Fig. 2; $V_{r.f.} = 0.5V_{r.f.,\,max}$) upon the initial r.f. phase angle θ and kinetic energy ε_{kin}.

the pseudopotential barrier and other conditions during injection were the same in both cases, so that we can compare their trapping efficiencies.

As in the case of the dependence on r.f. phase θ, the dependence of the trapping efficiency $P_{\varepsilon\theta}$ on initial kinetic energy is very complex. However, the range of energy for which ions can be trapped is very broad (from 3 to 47 eV in our case). Note that in this case the pseudopotential well depth D_z is equal to $\sim$17 eV, which corresponds to a pseudopotential barrier height (see Fig. 5) of 12.4 eV. The intervals of energies for which trapping efficiency is high (about unity) are

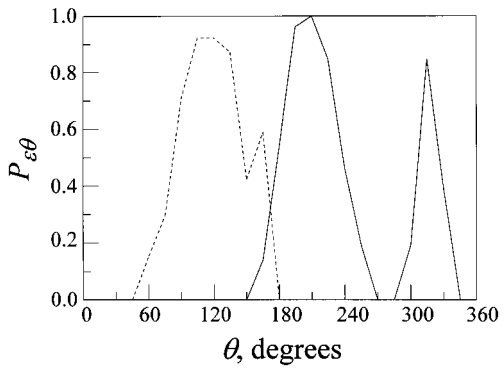

Figure 12. Dependence of the trapping efficiency $P_{\varepsilon\theta}$ during injection of m/z 1000 ions into an ion trap with increasing r.f. field (r.f. waveform as in Fig. 2; $V_{r.f.} = 0.5V_{r.f.,\,max}$) upon the initial r.f. phase angle θ for the initial kinetic energy $\varepsilon_{kin} = 21$ (solid line) and 40 eV (dashed line).

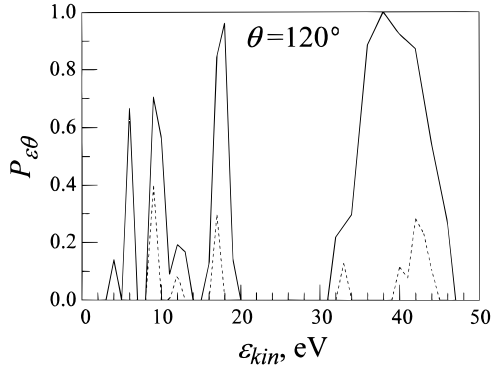

Figure 13. Dependence of the trapping efficiency $P_{\varepsilon\theta}$ upon the initial kinetic energy ε_{kin} at an r.f. phase angle $\theta = 120°$ for injection of m/z 1000 ions into a trap with increasing (r.f. waveform as in Fig. 2; $V_{r.f.} = 0.5V_{r.f.,\,max}$) (solid line) and constant (dashed line) r.f. field.

broad, so that the chance of trapping ions from the ion beam is always high if the beam is not monoenergetic (as is the case for MALDI). Two more conclusions following from the data shown in Fig. 13 are worthy of note. The first is that the trapping efficiency for injection into a constant r.f. field is not zero, even for the collisionless conditions we consider in this simulation. This conclusion is not actually new, because in the calculations of O and Schuessler[18] over certain narrow ranges of the r.f. phase, ions injected into a constant r.f. field were trapped over many milliseconds. The second interesting observation is that the dependence of the trapping efficiency on the initial kinetic energy in the case of injection into a constant r.f. field follows that for the case of injection into an increasing r.f. field. However, the peaks in the case of injection into a constant field are much narrower and lower than that in the case of an increasing r.f. field.

Averaging of the trapping efficiency over the r.f. voltage phase according to Eqn (4) is of practical interest, because the real ensemble of MALDI ions will be widely extended in time at the entrance into the trap. The result of such calculations for injection of m/z 1000 ions into an increasing r.f. field with $V_{r.f.} = 0.5V_{r.f., max}$ is shown in Fig. 14. The averaged trapping efficiency is normally between 0.19 and 0.3. This interval is even narrower (0.21–0.27) when the values for the trapping efficiency are smoothed over the energy interval of ± 4 eV. Such smoothing occurs experimentally as well because MALDI ions are not monoenergetic.[42–47] The results in Fig. 14 are considerably different from those obtained before averaging over θ (Fig. 11), where all dependences are very sharp. The low dependence of the averaged trapping efficiency P_ε on the initial kinetic energy predicted by these calculations was unexpected, but important in explaining the relative insensitivity of the molecular mass distributions in spectra of PEG 1000 upon the time of the laser firing (Figs 8 and 9). This weak dependence of the averaged trapping efficiency on initial kinetic energy cannot be obtained using the pseudopotential approximation approach alone, because in that approach the trapping efficiency is a strong function of the difference between the initial kinetic energy of an ion and the height of the pseudopotential barrier.

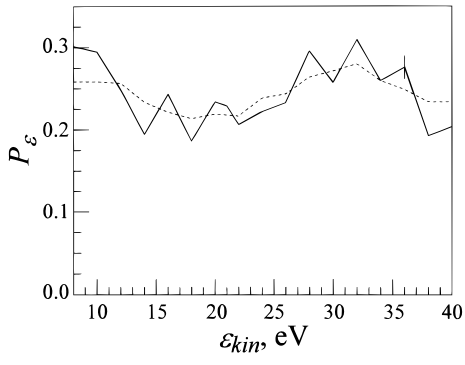

Figure 14. Dependence of the trapping efficiency P_ε averaged over the initial r.f. phase angle (solid line) upon the initial kinetic energy ε_{kin} for injection of m/z 1000 ions into a trap with increasing r.f. field (r.f. waveform as in Fig. 2; $V_{r.f.} = 0.5V_{r.f., max}$). The dashed line corresponds to the trapping efficiency P_ε smoothed over ±4 eV energy interval.

The dependences of the trapping efficiency P_ε, averaged over the r.f. phase, on the mass m of (singly charged) ions injected into an increasing r.f. field ($V_{r.f.} = 0.5V_{r.f., max}$) and having different initial kinetic energies (ε_{kin} = 18, 20, 22 and 24 eV) are shown in Fig. 15. In contrast to our previous calculations, the total time of flight of ions before entering the trap was simulated here, i.e. $t_{TOF} \propto (m/\varepsilon_{kin})^{1/2}$ with $t_{TOF} = 15$ μs for m/z 1000 ions having kinetic energy $\varepsilon_{kin} = 21$ eV. Although the trapping efficiencies for different masses and energies can differ by a factor of 2, the trapping efficiency averaged over all four energies (shown by the dashed line in Fig. 15) exhibits a slow increase from 0.2 to 0.27 when the mass is changed from 500 to 2000 Da. This means that (within an accuracy of 15–20%) the trapping efficiency is the same for all masses from 500 to 2000 Da, which is in good agreement with our experiment (Figs 6 and 7).

Model for the injection of ions into increasing and constant r.f. fields

The behavior of the trapping efficiency in cases in which ions are injected into increasing and constant r.f. fields can be used to build a common model for trapping ions injected into increasing and constant r.f. fields. Two observations are important in building this model. The first is the broad range of the initial kinetic energies for which trapping is possible in both cases (Fig. 13). The second is the similar behavior of the trapping efficiency in both cases upon the kinetic energy although the numerical values for the trapping efficiency are different.

The broad range (from 3 to 47 eV) of kinetic energies for which trapping is possible (in this study, when the pseudopotential barrier height is equal to 12.4 eV) and nearly constant trapping efficiency averaged over the r.f. voltage phase cannot be explained by the pseudopotential field approximation. Trapping at energies significantly lower or higher than the pseudopotential barrier height means that energy can be effectively acquired or lost during injection because ions are trapped only if their final total energies inside the trap (kinetic energy plus the pseudopotential) are lower than the pseudopotential well depth. (Again, the pseudopotential well approximation is valid inside the trap if

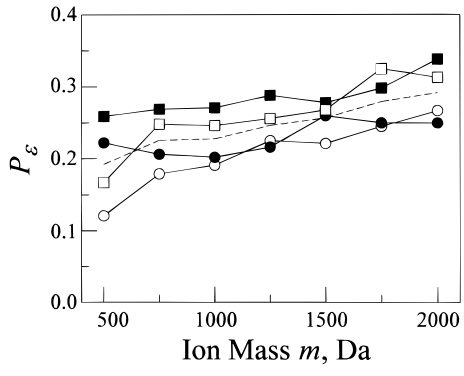

Figure 15. Dependence of the trapping efficiency P_ε averaged over the r.f. phase angle θ upon the mass m of ions injected into a trap with increasing r.f. field (r.f. waveform as in Fig. 2; $V_{r.f.} = 0.5V_{r.f., max}$) for different injection energies ε_{kin}: 18 eV (○), 20 eV (●), 22 eV (□) and 24 eV (■). The trapping efficiency shown by the dashed line is the average for all energies above.

$q_z < 0.4$). The similarity of behavior in the dependence of trapping efficiency on initial kinetic energy for ions injected into increasing or constant r.f. fields means that the mechanism for trapping is also similar for both of these cases.

As a result of our experimental and numerical study of the injection of ions into an ion trap, a simple model has been developed which qualitatively describes all of the phenomena observed and provides a better understanding of the trapping process. The model is equally suitable for explaining effects observed during injection of ions into both increasing and constant r.f. fields underscoring the common physics for trapping ions in both of this methods. For reasons that will (hopefully) become clear, we refer to this model as the 'swinging doors' model. The pseudopotential well approximation that has been shown to be useful in many cases, remains valid inside the trap if $q_z < 0.4$, which is true in most of the experiments including ours. However, this approximation is not valid in the narrow region adjacent to the trap electrodes including that near the holes in the end-cap electrodes. The width of this region is about the same as the amplitude of the micro-oscillations of ions at the fundamental r.f. frequency.

For our model, the process of trapping ions is separated into three stages: (A) injection of ions into the trap, (B) capture of the ions via phase interaction with the r.f. field (rather than via collisions with buffer gas molecules) for more than one cycle of secular oscillations (the frequency of these oscillations is determined by the r.f. voltage on the ring electrode and is much lower than that of the r.f. voltage) and (C) final trapping of ions via slow dissipation of ion energy in collisions with the buffer gas molecules. These stages are considered below in detail.

Stage A. This stage is identical for ions injecting into both an increasing or constant r.f. field and includes the period during which ions pass through the hole in the entrance end-cap electrode. This is the most important stage in the entire trapping process, because during this stage an ion can be reflected back from the trap or pass inside the trap, depending upon the energy it acquires from the r.f. field while approaching the hole and entering the trap. In this stage, the hole acts as a 'swinging door' which can increase or decrease ion energy or reflect the ion, depending upon whether the potential in the vicinity of the entrance hole is in or out of phase with the incoming ion. The 'swinging door' changes not only the ion energy but also its direction. As a result, an ion may be scattered over many different angles so that the direction of its velocity after this stage can be quite different, in some cases being reflected in the reverse direction. The magnitude of the change in ion energy at this stage is comparable to the initial kinetic energy and can even exceed the initial kinetic energy as shown from the data in Fig. 13. It is this change of energy that makes possible the primary trapping of the ions later at the stage B. The average kinetic energy transfer in collisions with buffer gas molecules is about $2M/m$ and in the case of m = 1000 Da and helium as the buffer gas (M = 4 Da) does not exceed 1%. Thus, any changes in energy due to the small number of collisions with buffer gas molecules (that are possible during the stages A and B) are negligible in comparison with that resulting from the interaction with the 'swinging door' at stage A.

Stage B. During this stage, ions entering the trap may or may not be captured in the trap during period which is typically about 10–40 μs. Successful trapping in this stage depends on whether the ion is reflected in its first pass from the exit end-cap electrode. Although successful trapping is determined by the difference between the total energy (kinetic plus pseudopotential) of the ion and the pseudopotential well depth, the manner in which the pseudopotential energy is built is different for ions injected into increasing or constant r.f. fields. In the case of the constant r.f. field, the pseudopotential well is not changed at this stage. Thus, the ion is trapped only if its total energy is less than the pseudopotential well depth. In the case of injection into an increasing r.f. field the pseudopotential well gets deeper while the ion is inside the trap. Thus, the chance of trapping ions is much higher in this case. This is the only (but very important) difference between the cases of ion injection into increasing and constant r.f. fields, which results in orders of magnitude differences for the trapping efficiency.

Stage C. Again, this stage is identical for injection of ions into both the increasing and constant r.f. field. The energy of trapped ions is slowly dissipated in collisions with the buffer molecules that normally occur over many milliseconds depending on the pressure of the buffer gas. The final ion distribution in the ion trap is determined by the ambient temperature and trap parameters[53] and the ionic environment.[54]

CONCLUSION

For the MALDI/ion trap interface developed in this work for external axial injection of ions into a trap with an increasing r.f. field, no or small mass discrimination was observed for the trapping of ions of poly(ethylene glycol) (PEG 1000 and 1500) in the wide mass range of 500–2000 Da and for a broad range of experimental conditions which included initial kinetic energies of 5–40 eV and r.f. voltages of 400–4000 V_{0-p} ramped at the rate of 30–140 V_{0-p} μs^{-1}.

Numerical simulations showed sharp dependences of the trapping efficiency upon the initial kinetic energy of ions and r.f. voltage phase. However, after the averaging over the r.f. voltage phase and energy interval normally associated with the MALDI process the trapping efficiency is relatively constant (within 15–20%) and high (normally 0.2–0.3) for conditions corresponding to the experiment. The high trapping efficiency calculated in this work for trapping ions by increasing the r.f. voltage is in a good agreement with experiment[37] in which an order of magnitude improvement was observed for trapping ions using this method in comparison with that for ion injection into a constant r.f. field. Our numerical simulation showed the importance of taking into account the holes in the end-cap electrodes that results in the essentially two-dimensional structure for ion motion inside the trap and a corresponding increase for the trapping efficiency which cannot be observed if ion

trajectories in the simulation are originated from a trap electrode surface.[19,34] The two-dimensional structure of ion motion was not also taken into account by Qin and Chait[36] during interpretation of their experiment for measuring the trapping efficiency. The importance of the interaction between injected ions and the r.f. field and the relative unimportance of collisions with buffer gas molecules for trapping ions shown in this work for the case of injection into a constant and slowly increasing r.f. field, are in line with the results of the experiment[35] and numerical simulation[17–19] for phase-synchronized pulsed injection of ion beams of very short duration into the trap.

As the result of the experiments and numerical simulation, a simple 'swinging door' model has been developed for qualitative description of the process of ion injection into the trap. The trapping process in this model is separated onto three stages. In the first, the hole in the entrance end-cap electrode acts as a 'swinging door' resulting in an increase in ion kinetic energy if the ion and 'door' are in-phase, or a decrease in energy if they are out-of-phase. At the second stage ions are (or are not) captured by the r.f. field depending on the ion energy after the first stage and the pseudopotential well depth of the r.f. field. The fate of ions in the second stage is determined during a period lasting tens of microseconds. Collisions with buffer molecules are not important during the first and second stages. Finally, during a third stage lasting many milliseconds, the energy of ions is lost in the dissipative process via collisions with buffer molecules. The model is equally applicable for ion injection into both the increasing and constant r.f. field. The only, but very important, difference between these two cases is the way in which the pseudopotential energy is built during the second stage. For ions injected into an increasing r.f. field the pseudopotential barrier height increases while the ions are inside the trap. Hence the chance of trapping ions is much higher in this case. This results in orders of magnitude difference for the trapping efficiency for these cases.

Acknowledgements

This work was supported in part by a grant from the National Institutes of Health (R01 RR08912) and carried out at the Middle Atlantic Mass Spectrometry Laboratory.

REFERENCES

1. W. Paul and H. Steinwedel, Ger. Pat. 944900 (1956); US Pat. 2939952 (1960).
2. R. E. March and R. J. Hughes, *Quadrupole Storage Mass Spectrometry*. Wiley, New York (1989).
3. P. Kofel, in *Practical Aspects of Ion Trap Mass Spectrometry*, edited by R. E. March and J. F. J. Todd, Vol. 2, p. 51. CRC Press, New York (1995).
4. P. E. Kelley, G. C. Stafford, Jr, and D. R. Stephens, US Pat. 5540884 (1985).
5. J. N. Louris, J. W. Amy, T. Y. Ridley and R. G. Cooks, *Int. J. Mass Spectrom. Ion Processes* **88**, 97 (1989).
6. R. E. Kaiser, Jr, J. N. Louris, J. W. Amy and R. G. Cooks, *Rapid Commun. Mass Spectrom.* **3**, 225 (1989).
7. S. A. McLuckey, G. L. Glish and K. G. Asano, *Anal. Chim. Acta* **225**, 25 (1989).
8. G. J. Van Berkel, G. L. Glish and S. A. McLuckey, *Anal. Chem.* **62**, 1284 (1990).
9. D. N. Heller, I. Lys, R. J. Cotter and O. M. Uy, *Anal. Chem.* **61**, 1083 (1989).
10. G. L. Glish, D. E. Goeringer, K. G. Asano and S. A. McLuckey, *Int. J. Mass Spectrom. Ion Processes* **94**, 15 (1989).
11. K. A. Cox, J. D. Williams, R. J. Cooks and R. E. Kaiser, Jr, *Biol. Mass Spectrom.* **21**, 226 (1992).
12. V. M. Doroshenko, T. J. Cornish and R. J. Cotter, *Rapid Commun. Mass Spectrom.* **6**, 753 (1992).
13. D. M. Chambers, D. E. Goeringer, S. A. McLuckey and G. L. Glish, *Anal. Chem.* **65**, 14 (1993).
14. K. Jonscher, G. Currie, A. L. McCormack and J. R. Yates, III, *Rapid Commun. Mass Spectrom.* **7**, 20 (1993).
15. J. C. Schwartz and M. E. Bier, *Rapid Commun. Mass Spectrom.* **7**, 27 (1993).
16. E. Fischer, *Z. Phys.* **156**, 1 (1959).
17. P. K. Ghosh, A. S. Arora and L. Narayan, *Int. J. Mass Spectrom. Ion Phys.* **23**, 237 (1977).
18. C.-S. O and H. A. Schuessler, *J. Appl. Phys.* **52**, 1157 (1981).
19. C. Weil, M. Nappi, C. D. Cleven, H. Wollnik and R. G. Cooks, *Rapid Commun. Mass Spectrom.* **10**, 742 (1996).
20. J. F. J. Todd, *Mass Spectrom. Rev.* **10**, 3 (1991).
21. S. A. McLuckey, G. J. Van Berkel, D. E. Goeringer and G. L. Glish, *Anal. Chem.* **66**, 689A (1994).
22. V. M. Doroshenko and R. J. Cotter, *Rapid Commun. Mass Spectrom.* **7**, 822 (1993).
23. A. McIntosh, T. Donovan and J. Brodbelt, *Anal. Chem.* **64**, 2079 (1992).
24. P. H. Dawson and N. R. Whetten, *US Pat.* 3521939 (1970).
25. M. N. Kishore and P. K. Ghosh, *Int. J. Mass Spectrom. Ion Phys.* **29**, 345 (1979).
26. J. F. J. Todd, D. A. Freer and R. M. Waldren, *Int. J. Mass Spectrom. Ion Phys.* **36**, 371 (1980).
27. C.-S. O and H. A. Schuessler, *Int. J. Mass Spectrom. Ion Phys.* **40**, 53 (1981).
28. C.-S. O and H. A. Schuessler, *Int. J. Mass Spectrom. Ion Phys.* **40**, 67 (1981).
29. C.-S. O and H. A. Schuessler, *Int. J. Mass Spectrom. Ion Phys.* **40**, 77 (1981).
30. N. Watanabe, H. Shiromaru, N. Kurihara, Y. Achiba, N. Kobayashi, Y. Kaneko and J. Yoda, *Nucl. Instrum. Methods Phys. Res.* **B69**, 385 (1992).
31. V. M. Doroshenko and R. J. Cotter, in *Laser Ablation: Mechanisms and Applications – II*. Proceedings of the 2nd International Conference on Laser Ablation, Knoxville, TN, 19–22 April 1993, edited by J. C. Miller and D. B. Geohegan, p. 513. AIP Press, New York (1994).
32. V. M. Doroshenko and R. J. Cotter, US Pat. 5399857 (1995).
33. G. C. Eiden, M. E. Cisper, M. L. Alexander and P. H. Hemberger, *J. Am. Soc. Mass Spectrom.* **4**, 706 (1993).
34. G. C. Eiden, A. W. Garrett, M. E. Cisper, N. S. Nogar and P. H. Hemberger, Int. *J. Mass Spectrom. Ion Processes* **136**, 119 (1994).
35. J. E. Crawford, F. Buchinger, L. Davey, Y. Ji, J. K. P. Lee, J. Pinard, J. L. Vialle and W. Z. Zhao, Hyperfine Interact. **81**, 143 (1993).
36. J. Qin and B. T. Chait, *Anal. Chem.* **68**, 2102 (1996).
37. A. W. Garrett, M. E. Cisper, N. S. Nogar and P. H. Hemberger, *Rapid Commun. Mass Spectrom.* **8**, 174 (1994).
38. D. A. Dahl, *SIMION 3D Version 6.0 User's Manual*. Princeton Electronic Systems, Princeton, NJ (1995).
39. V. M. Doroshenko and R. J. Cotter, *Rapid Commun. Mass Spectrom.* **10**, 65 (1996).
40. V. M. Doroshenko and R. J. Cotter, *Anal. Chem.* **68**, 463 (1996).
41. V. M. Doroshenko and R. J. Cotter, *Rapid Commun. Mass Spectrom.* **8**, 766 (1994).
42. B. Spengler and R. J. Cotter, *Anal. Chem.* **62**, 793 (1990).

43. W. Ens, Y. Mao, F. Mayer and K. G. Standing, *Rapid Commun. Mass Spectrom.* **5**, 117 (1991).
44. T. Huth-Fehre and C. H. Becker, *Rapid Commun. Mass Spectrom.* **5**, 378 (1991).
45. R. C. Beavis and B. T. Chait, *Chem. Phys. Lett.* **181**, 479 (1991).
46. Y. Pan and R. J. Cotter, *Org. Mass Spectrom.* **27**, 3 (1992).
47. J. Zhou, W. Ens, K. G. Standing and A. Verentchikov, *Rapid Commun. Mass Spectrom.* **6**, 671 (1992).
48. F. G. Major and H. G. Dehmelt, *Phys. Rev.* **179**, 91 (1968).
49. A. V. Gaponov and M. A. Miller, *Zh. Eksp. Teor. Fiz.* **34**, 242 (1958).
50. R. J. Cotter, *Anal. Chem.* **64**, 1027A (1992).
51. U. Bahr, A. Deppe, M. Karas, F. Hillenkamp and U. Giessmann, *Anal. Chem.* **64**, 2866 (1992).
52. C. G. de Koster, M. C. Duursma, G. J. Van Rooij, R. M. A. Heeren and J. J. Boon, *Rapid Commun. Mass Spectrom.* **9**, 957 (1995).
53. S. Guan and A. G. Marshal, *J. Am. Soc. Mass Spectrom.* **5**, 64 (1994).
54. G. A. Bach, E. A. Dynin and N. J. Kirchner, In *Proc. 43rd ASMS Conference on Mass Spectrometry and Allied Topics*, Atlanta, GA, 21–26 May, 1995, p. 1108.